Original Article

Institution of MECHANICAL ENGINEERS
Journal of MECHANICAL ENGINEERING SCIENCE

Proc IMechE Part C:
J Mechanical Engineering Science
0(0) 1–15

DOI: 10.1177/0954406216638883
pic.sagepub.com
SAGE

Unilateral contact condition enhanced with squeeze film modelling in automotive differentials

Geoffrey Virlez[1], Olivier Brüls[1], Pierre Duysinx[1], Michel Géradin[1,2] and Alberto Cardona[3]

Abstract

The dynamic behaviour of automotive drivetrains is significantly influenced by contacts occurring between the various parts. In this paper, a three-dimensional formulation is proposed to model unilateral and frictional contact conditions between two rigid planar rings. The magnitude of the contact force is determined by a penalty method. In a second step, a simple squeeze film model is developed to account for the damping effect produced by the lubricating oil filling the gap between the two contacting bodies. The relevance and the accuracy of these models are illustrated through the global multibody modelling of a TORSEN differential.

Keywords

Squeeze film, rigid contact model, automotive differential, dynamic multibody system

Date received: 4 May 2015; accepted: 16 February 2016

Introduction

Virtual prototyping is more and more used in the automotive industry in order to improve the performance of each component and reduce the fuel consumption. Global models are often required owing to the complexity and the numerous interactions between the various subsystems of modern vehicles. In this context, the development of reliable and accurate models of the driveline is required in order to fully model the car from the engine[1] to the vehicle dynamics.[2] However, the numerical simulation of transmission components such as gear box, clutch or differential is not trivial since complex physical phenomena[3] are involved (clearance, misalignment, flexibility, friction, lubrication, impact,...) and can highly influence the dynamic response of the whole vehicle.

In this work, the TORSEN (TORque SENsing) differential has been chosen as a representative industrial application to assess some of the difficulties inherent to the development of global multibody models to simulate the dynamics of driveline devices.

After a technical description of the principle of working of TORSEN differentials, the nonlinear finite element method for flexible multibody systems is briefly recalled. In the frame of this simulation approach, the mathematical formulation will be looked over for the two main kinematic joints used in the model of TORSEN differentials: the gear pair element and the contact condition.

The first models achieved with the MECANO module of the commercial software LMS SAMTECH SAMCEF[4] (referred to as SAMCEF MECANO in the remainder of the paper) have shown the essential role played by the contact formulation in the modelling of this particular transmission component. Several limitations have been identified and the need appears to develop a three-dimensional (3D) contact formulation between two rigid bodies which is able to deal with impact phenomena. For this reason, this paper is dedicated to the development of enhanced contact modelling approaches between rigid bodies.

In a first step, the magnitude of the contact force is determined by a continuous impact law where a restitution coefficient accounts for the kinetic energy loss

[1]Department of Aerospace and Mechanical Engineering (LTAS), University of Liège, Belgium
[2]Humboldt Research Awardee, TUM, Germany
[3]Universidad Nacional del Litoral – CONICET, CIMEC, Santa Fe, Argentina

Corresponding author:
Geoffrey Virlez, Department of Aerospace and Mechanical Engineering (LTAS), University of Liège, Quartier Polytech 1, Allée de la Découverte 9 (B52/3), Liège 4000, Belgium.
Email: g.virlez@gmail.com

during the impact. A regularisation method is also used to compute both the normal and the friction forces.

Then, a squeeze film model is proposed to represent the damping effect produced by the presence of lubricant between approaching bodies. Indeed, the presence of lubricant between drivetrain components modifies the contact properties in a non-negligible way.[5,6] The dynamics of unilateral contacts is modified in both normal and tangential directions. The developed model has a very compact formulation thanks to the geometrical assumptions adopted.

In both cases, an engineer approach is preferred to a detailed 3D representation of the contact, which could be more accurate but would be highly expensive from a computational point of view and not feasible in practice for global industrial applications.[7] The relevance of the model is demonstrated with the modelling of the interaction between the gear wheels and the thrust washers in the type C TORSEN differential. The comparison of the numerical results with experimental data enables to validate the multibody model in a global way. Finally, it is observed that thanks to the combined squeeze film – contact model, the TORSEN differential model has gained robustness and computational efficiency, so that it can be included in a full vehicle model in order to simulate various manoeuvres.

Technical description of TORSEN differentials

The two essential functions of a differential are to transmit the motor torque to the two output shafts and to allow a difference of rotation speed between these two outputs. In a vehicle, this mechanical device is particularly useful in cornering when the outer wheels have to rotate quicker than the inner wheels to ensure a good handling. The differential can be used either to divide the drive torque into equal parts acting on the traction wheels of the same axle, or to divide the output torque from the gearbox between the two axles of a four-wheel drive vehicle. This second application is often called the transfer box differential or central differential.

The main drawback of a conventional differential (open differential) is that the total amount of available torque is always split between the two output shafts with the same constant ratio. The TORSEN differentials significantly reduce this undesirable side effect. This kind of limited slip differential allows a variable distribution of motor torque depending on the available friction of each driving wheel.

When a TORSEN differential is used, the torque biasing is always a precondition before any difference of rotation speed between the two output shafts. Contrary to viscous coupling, TORSEN is an instantaneous and pro-active process which acts before wheel slip.

The type C TORSEN differential has been fully modelled in this work. As depicted in Figure 1, this central differential is mainly composed of an epicyclic gear train, several thrust washers and a housing split in two parts. The friction generated by the contact between the planet gears and the housing as well as between the gear wheels and the thrust washers is at the origin of the locking effect and torque transfer of TORSEN differentials. This limited slip differential has four working modes which depend on the direction of torque biasing and on the drive or coast situation. Depending upon the active mode, the gear wheels rub against one or the other thrust washers which can have different friction coefficients and contact surfaces. Therefore, the locking rate is different for each working mode and is directly related to the total friction torque involved.

We note that the type B and type C TORSEN differentials are not axially prestressed. The lock nut only enables to close the differential and to fix the case with the housing, since axial loads applied by the helical gear pairs always try to separate these two parts. Even when the lock nut is completely screwed against the case stop, small gaps remain between the thrust washers and the gear wheels, which are at the origin of impact phenomena.

Flexible multibody simulation approach

In this work, the approach chosen to model the TORSEN differential is based on the nonlinear finite element method for flexible multibody systems.[8] This method allows the modelling of complex mechanical systems composed of rigid and flexible bodies, kinematics joints and force elements. Absolute nodal coordinates are used with respect to an inertial frame for each node of the model. Hence, there is no distinction between rigid and elastic coordinates which allows accounting in a natural way for many nonlinear flexible effects and large deformations. The Cartesian rotation vector combined with an updated Lagrangian approach is used for the parameterisation of rotations. This choice enables the representation of large rotations.

The dynamics of a system including holonomic bilateral constraints is described by equations (1) and (2)

$$\boldsymbol{M}(\boldsymbol{q})\,\ddot{\boldsymbol{q}} + \boldsymbol{g}(\boldsymbol{q},\dot{\boldsymbol{q}},t) + \boldsymbol{\Phi}_{\boldsymbol{q}}^{T}(\,p\boldsymbol{\Phi} + k\lambda) = \boldsymbol{0} \tag{1}$$

$$k\,\boldsymbol{\Phi}(\boldsymbol{q},t) = \boldsymbol{0} \tag{2}$$

where $\boldsymbol{q}$, $\dot{\boldsymbol{q}}$ and $\ddot{\boldsymbol{q}}$ are the generalsed displacements, velocities and acceleration coordinates, $\boldsymbol{M}(\boldsymbol{q})$ is the mass matrix, $\boldsymbol{g}(\boldsymbol{q},\dot{\boldsymbol{q}},t) = \boldsymbol{g}^{gyr}(\boldsymbol{q},\dot{\boldsymbol{q}}) + \boldsymbol{g}^{int}(\boldsymbol{q},\dot{\boldsymbol{q}}) - \boldsymbol{g}^{ext}(t)$ is a global forces vector where $\boldsymbol{g}^{gyr}$ states for the complementary inertia forces, $\boldsymbol{g}^{int}(\boldsymbol{q},\dot{\boldsymbol{q}})$ the internal forces, e.g. contact, elastic and dissipation forces, and $\boldsymbol{g}^{ext}(t)$

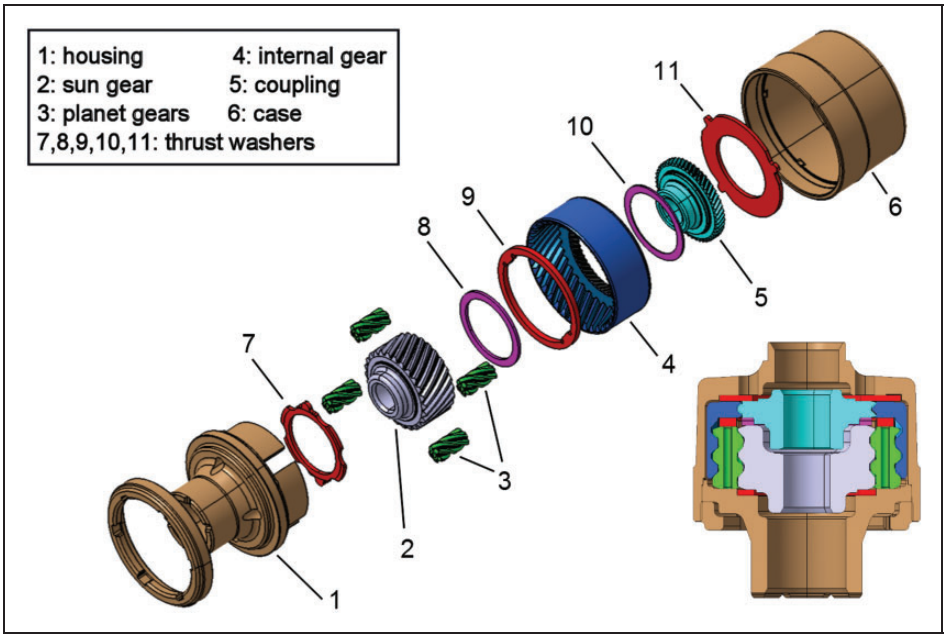

Figure 1. Exploded view and cut-away view of type C TORSEN differential.

the external forces. According to the augmented Lagrangian method, the constraint forces are formulated by $\boldsymbol{\Phi}_{\boldsymbol{q}}^{T}(p\boldsymbol{\Phi}+k\lambda)$ where λ is the vector of Lagrange multipliers related to algebraic constraints $\boldsymbol{\Phi}=\boldsymbol{0}$; p and k are respectively a penalty factor to enforce the constraints and a scaling factor to improve their numerical conditioning; $\boldsymbol{\Phi}_{\boldsymbol{q}}$ is the constraint gradient $(\partial\boldsymbol{\Phi}/\partial\boldsymbol{q})$.

Equations (1) and (2) form a system of nonlinear differential-algebraic equations. The solution is evaluated step by step using the generalized α-method which allows adding numerical damping to the time integration scheme while preserving its second-order accuracy.[9,10] At each time step, a system of nonlinear algebraic equations has to be solved using a Newton-Raphson iteration process.

Global gear pair model

The two main kinematic constraints needed to model TORSEN differentials are the gear pair and the contact conditions with the housing and the thrust washers. A dedicated global gear pair model is available in SAMCEF MECANO for describing flexible gear pairs in the 3D analysis of flexible mechanisms.[11,12] It is a global kinematic joint defined between two physical nodes: one at the centre of both gear wheels, the latter being represented as rigid bodies. The flexibility of the gear mesh is accounted for by a nonlinear spring and damper element inserted along the instantaneous normal pressure line. Several specific phenomena in gear pairs can also be taken into account in the model, namely backlash, mesh stiffness fluctuation, friction between teeth. The lubrication between contacting gear teeth was not considered in this model. Nevertheless, it is a second-order effect which could be implemented in future work.

Unilateral rigid/flexible contact condition

In order to model the unilateral contacts between the lateral face of the gear wheels and the thrust washers of the TORSEN differential, a rigid/flexible contact condition based on kinematic constraints[13] has been used during the first modelling stage. The gear wheels are modelled as rigid bodies, whereas the thrust washers are flexible bodies represented with volume finite elements.

The contact conditions are created between a set of nodes on the flexible body that will be connected to a surface of the rigid body. The contact algorithm consists of two steps: the first one consists in searching the projection of each slave node in the master surface and creating an associated distance sensor and in the second step, the kinematic constraint is imposed. In the nonlinear case (large displacements, large rotations), the contact is treated together with the other nonlinearities and a coupled iteration method is used.[13]

In case of convergence problems, the use of a penalty function allows small penetration between the bodies in contact. Physically, this penalty function behaves as a spring that is active in compression but not in traction. Damping is sometimes used to smooth the response and consequently get better convergence properties.

The friction has to be taken into account in all contact conditions since friction plays a key role in the working principle of TORSEN differentials. Therefore, in addition to the distance sensor,

sliding sensors are also generated. The friction force F_{fr} is directly proportional to the normal reaction between the slave node and the master surface by means of a regularized friction coefficient μ_R ($F_{fr} = \mu_R |F_{norm}|$). A regularisation tolerance is used to avoid the discontinuity of the friction force when the relative sliding velocity vanishes.

A dynamic analysis of the TORSEN differential has been achieved in previous works.[14,15] The comparison of the torque distribution ratios (TDR) provided by the numerical simulation with experimental data permits to globally validate the model. However, several drawbacks mainly due to the formulation of the contact conditions have been identified in the simulation of this industrial application. Indeed, the contact formulation using algebraic constraints at position level has a poor robustness. The model based on a penalty method permits the convergence if sufficiently small time steps are used. Nevertheless, the contact element remains highly sensitive to the value of the contact stiffness and other parameters such as the numerical damping. Moreover, the aforementioned contact formulation requires that at least one of the contacting bodies is flexible. However, for the application under study, it is not essential to account for the flexibility of all the bodies in contact. The rigid–flexible contact element complicates unnecessarily the model, increases its size and makes the simulation CPU time expensive. This has motivated the development in the sequel of this paper of a contact element between two rigid bodies which turns out be better adapted to impact simulation.

Kinematics of the contact between two rigid planar rings

This section describes a kinematic formulation able to model the normal contact forces and the tangent friction forces between two rigid planar rings. This configuration occurs, for instance, for the contacts between the gear wheels and the thrust washers of TORSEN differentials. This contact element allows to simulate unilateral contacts when the contacting bodies are subjected to large displacements and rotations in 3D analysis. The formulation fits into a nonlinear finite element framework and has been implemented as a *user element* in the multibody software SAMCEF MECANO.

As for most contact models between rigid bodies, the proposed contact element is defined between two nodes fixed on the two rigid bodies potentially in contact. These nodes A and B are not necessarily located at the centre of gravity of the two bodies but are the origins of two material frames (namely $\{A; \boldsymbol{e}''_{A_1}, \boldsymbol{e}''_{A_2}, \boldsymbol{e}''_{A_3}\}$ and $\{B; \boldsymbol{e}''_{B_1}, \boldsymbol{e}''_{B_2}, \boldsymbol{e}''_{B_3}\}$) following the rigid body motion.

In the initial configuration, these material frames denoted by the vectors $\boldsymbol{e}_{A_i}$ and $\boldsymbol{e}_{B_i}$ are chosen parallel for simplicity. The rotation matrix $\boldsymbol{R}_1$ gives the initial orientation of both material frames with respect to the inertial frame $\{O; \boldsymbol{E}_1, \boldsymbol{E}_2, \boldsymbol{E}_3\}$:

$$\boldsymbol{e}_{A_i} = \boldsymbol{R}_1 \, \mathbf{E}_i \tag{3}$$

$$\boldsymbol{e}_{B_i} = \boldsymbol{R}_1 \, \mathbf{E}_i \tag{4}$$

The rotation operators $\boldsymbol{R}_A$, $\boldsymbol{R}_B$ enable to compute the rotation from initial to current configuration (equations (5) and(6).

$$\boldsymbol{e}''_{A_i} = \boldsymbol{R}_A \, \boldsymbol{e}_{A_i} = \boldsymbol{R}_A \, \boldsymbol{R}_1 \, \boldsymbol{E}_i \tag{5}$$

$$\boldsymbol{e}''_{B_i} = \boldsymbol{R}_B \, \boldsymbol{e}_{B_i} = \boldsymbol{R}_B \, \boldsymbol{R}_1 \, \boldsymbol{E}_i \tag{6}$$

The magnitude and the direction of the contact and friction forces depend on the instantaneous relative position and orientation of both material frames. Therefore, the force vectors will be first computed according to the relative position and rotation vectors expressed in the material frame attached to node A. Afterwards, these force vectors will be expressed in the inertial frame.

The relative position vector $\boldsymbol{u}$ of node B with respect to node A in the frame $\{A; \boldsymbol{e}''_{A_1}, \boldsymbol{e}''_{A_2}, \boldsymbol{e}''_{A_3}\}$ can be easily computed from the fundamental equation describing the rigid body kinematics

$$\boldsymbol{u} = \boldsymbol{R}_1^T \boldsymbol{R}_A^T (\boldsymbol{x}_B - \boldsymbol{x}_A) \tag{7}$$

where $\boldsymbol{x}_A, \boldsymbol{x}_B$ are the position coordinates of nodes A and B in the inertial frame.

The vectors $\boldsymbol{e}''_{B_i}$ are defined in the inertial frame but can also be expressed in the frame $\{A; \boldsymbol{e}''_{A_1}, \boldsymbol{e}''_{A_2}, \boldsymbol{e}''_{A_3}\}$:

$$\boldsymbol{e}''_{B_i/A} = (\boldsymbol{R}_A \boldsymbol{R}_1)^T \, \boldsymbol{e}''_{B_i} = \boldsymbol{R}_1^T \boldsymbol{R}_A^T \boldsymbol{R}_B \boldsymbol{R}_1 \, \mathbf{E}_i = \boldsymbol{R}_{rel} \, \mathbf{E}_i \tag{8}$$

where $\boldsymbol{R}_{rel}$ is the relative rotation matrix.

Since the contact model is defined between the nodes A and B, the generalised coordinates vector $\boldsymbol{q}$ of the contact element is simply composed of the set of position coordinates $\boldsymbol{x}_A, \boldsymbol{x}_B$ and rotation parameters $\boldsymbol{\Psi}_{A\,inc}, \boldsymbol{\Psi}_{B\,inc}$ of the incremental rotation with respect to the previous converged rotation (updated Lagrangian formulation)[8]

$$\boldsymbol{q} = \begin{Bmatrix} \boldsymbol{x}_A \\ \boldsymbol{\Psi}_{A\,inc} \\ \boldsymbol{x}_B \\ \boldsymbol{\Psi}_{B\,inc} \end{Bmatrix} \tag{9}$$

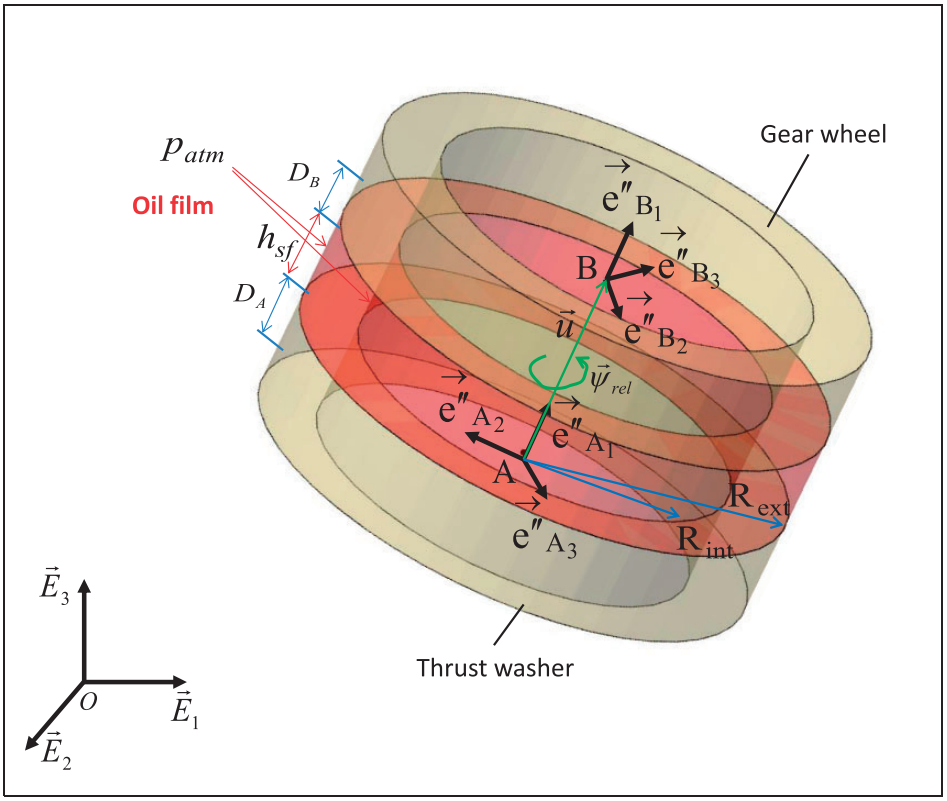

Figure 2. Kinematics of the contact between two planar rings.

Note that this set of coordinates is mixed, in the sense that position coordinates are expressed in the inertial frame, while rotation parameters are expressed in a frame local to each node giving the rotation at the previous computed time step.

The contribution vector $\boldsymbol{g}_{int}^{con}$ of the contact element to the internal forces of the multibody system is obtained by identification between the two expressions of the virtual work stated in the equation

$$\delta W = \delta \boldsymbol{q}^T \, \boldsymbol{g}_{int}^{con}(\boldsymbol{q}, \dot{\boldsymbol{q}}) = \delta \boldsymbol{u}^T \, \boldsymbol{f}_t + \delta \boldsymbol{\Theta}_{rel}^T \boldsymbol{f}_r \tag{10}$$

where the vectors $\boldsymbol{f}_t$ and $\boldsymbol{f}_r$ represent the contact forces and torques expressed in the material frame attached to node A.

The variations $\delta \boldsymbol{u}$, $\delta \boldsymbol{\Theta}_{rel}$ of the relative displacement and material relative rotation are computed by deriving the expressions (7) and (8)

$$\delta \boldsymbol{u} = \tilde{\boldsymbol{u}} \boldsymbol{R}_1^T \, \delta \boldsymbol{\Theta}_A + \boldsymbol{R}_1^T \boldsymbol{R}_A^T \, (\delta \boldsymbol{x}_B - \delta \boldsymbol{x}_A) \tag{11}$$

$$\delta \boldsymbol{\Theta}_{rel} = \boldsymbol{R}_1^T \, \delta \boldsymbol{\Theta}_B - \boldsymbol{R}_1^T \boldsymbol{R}_B^T \boldsymbol{R}_A \, \delta \boldsymbol{\Theta}_A \tag{12}$$

where $\tilde{\boldsymbol{u}}$ is the skew-symmetric matrix with components $(\tilde{\boldsymbol{u}})_{ij} = -\epsilon_{ijk} u_k$, and $\delta \boldsymbol{\Theta}_A, \delta \boldsymbol{\Theta}_B$ are material variations of the rotations at nodes A and B .

The quasi-coordinates $\delta \boldsymbol{\Theta}$ and the incremental Cartesian rotation parameters $\delta \boldsymbol{\Psi}_{inc}$ satisfy a tangential relationship[8]

$$\delta \boldsymbol{\Theta} = \boldsymbol{T}(\boldsymbol{\Psi}_{inc}) \, \delta \boldsymbol{\Psi}_{inc} \tag{13}$$

By identification between the two members of equation (10), the internal force vector due to each contact can be formulated as

$$\boldsymbol{g}_{int}^{con}(\boldsymbol{q}, \dot{\boldsymbol{q}}) = \boldsymbol{B} \begin{Bmatrix} \boldsymbol{f}_t \\ \boldsymbol{f}_r \end{Bmatrix} \tag{14}$$

where the matrix $\boldsymbol{B}$ is defined by

$$\boldsymbol{B} = \begin{bmatrix} -\boldsymbol{R}_A \boldsymbol{R}_1 & \boldsymbol{0} \\ -\boldsymbol{T}^T(\boldsymbol{\Psi}_{A\,inc}) \boldsymbol{R}_1 \tilde{\boldsymbol{u}} & -\boldsymbol{T}^T(\boldsymbol{\Psi}_{A\,inc}) \boldsymbol{R}_A^T \boldsymbol{R}_B \boldsymbol{R}_1 \\ \boldsymbol{R}_A \boldsymbol{R}_1 & \boldsymbol{0} \\ \boldsymbol{0} & \boldsymbol{T}^T(\boldsymbol{\Psi}_{B\,inc}) \boldsymbol{R}_1 \end{bmatrix} \tag{15}$$

The contribution of the contact force (14) to the iteration matrix is detailed in Virlez.[16]

The kinematic relations (3) to (8) and the nodal forces (14) computed are valid for any 3D contact between two rigid bodies. However, due to the modelling assumptions adopted in the TORSEN differential model, only the geometric configuration of two planar and coaxial rings remaining parallel has been numerically simulated (i.e. the relative motion is limited to a translation and a rotation along the normal direction).

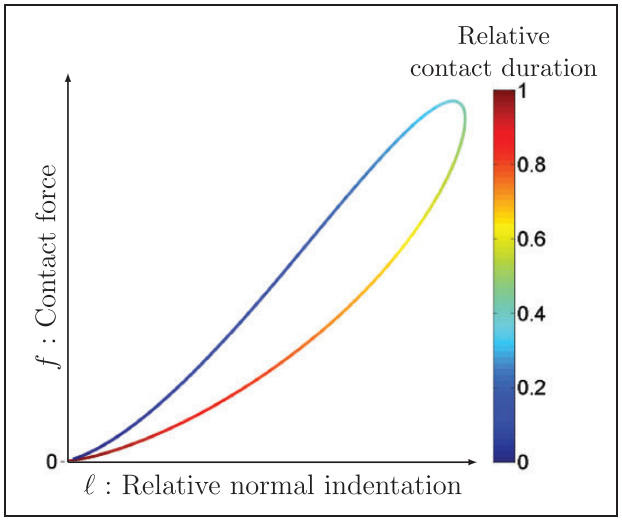

Figure 3. The area encircled by the hysteresis loop represents the kinetic energy loss due to the force law of the continuous impact model.

With these geometric assumptions, the contact forces and torques $\boldsymbol{f}_t, \boldsymbol{f}_r$ are reduced to the following expressions

$$\boldsymbol{f}_t = \begin{Bmatrix} -f \\ 0 \\ 0 \end{Bmatrix} \quad , \quad \boldsymbol{f}_r = \begin{Bmatrix} T_{fr} \\ 0 \\ 0 \end{Bmatrix} \tag{16}$$

where f is the magnitude of the normal contact force and T_{fr} is the magnitude of the friction torque.

The kinematics of the contact in this situation is depicted in Figure 2. The nodes A and B are located on the revolution axis of the rigid rings at a normal distance D_A or D_B from the contact surface. The first vector of the material frames is the normal direction of the contact force.

Continuous impact modelling

This section presents a first attempt to model contacts and impacts between rigid bodies in a multibody system.

The continuous impact model theory[17] enables to compute the magnitude of the normal contact force f. It is a penalty method based on a kind of Hertz law which uses the penetration ℓ as a representation of the local deformation of the two bodies in contact. The contact model has for expression

$$f(\ell, \dot{\ell}) = \begin{cases} k_p\, \ell^n + c\, \ell^n\, \dot{\ell} & \text{if} \quad \ell > 0 \\ 0 & \text{if} \quad \ell \leqslant 0 \end{cases} \tag{17}$$

with the contact stiffness k_p, which controls the stiffness like term. The model also includes a damping like term which accounts for the kinetic energy loss during the impact process (see Figure 3). This loss of energy is described by the damping parameter c which is related to the restitution coefficient e to the contact stiffness k_p and to the shapes and material properties of the colliding bodies as well as their relative velocities. The restitution coefficient e can take any value between 0 (plastic contact) and 1 ($c = 0$, no energy loss) and is defined as the norm of the relative velocity ratio after and before the impact. In order to avoid a jump at the beginning of the contact and tension force at the end, the viscous damping term $c\,\dot{l}$ is multiplied by l^n. The exponent n is equal to 1.5 for circular and elliptic contact areas.

According to the contact configuration, various expressions can be found in Lankarani and Nikravesh [18] for the damping parameter c. In this work, the empirical formula proposed by Flores et al.[19] has been used

$$c = \frac{8(1-e)}{5\,e}\frac{k_p}{\dot{l}_s} \tag{18}$$

where $\dot{l}_s$ is the relative normal velocity between bodies at the impact time. This expression has the advantage of being usable whatever be the amount of energy dissipation while most other definitions of the damping parameter c are only valid for high values of the restitution coefficient ($e > 0.8$).

The penetration length ℓ is easily determined thanks to the simple geometric configuration of the contact between two parallel rings

$$\ell = -\left(\boldsymbol{x}_{AB}^T\, \boldsymbol{n} - D_A - D_B\right) = -(u_1 - D_A - D_B) \tag{19}$$

where $\boldsymbol{x}_{AB} = \boldsymbol{x}_B - \boldsymbol{x}_A$ (see Figure 2). The penetration velocity is equal to minus the normal component of the relative velocity vector $\dot{\ell} = -\dot{u}_1$.

The magnitude of the friction force in the tangent plane is simply obtained by multiplying the normal contact force f by a regularised friction coefficient μ_R. The friction torque T_{fr} produced by the contact between the two rigid rings is thus computed as

$$T_{fr} = \int_S \mu_R\, p\, r\, \mathrm{d}S = 2\pi\, \mu_R\, \frac{f}{S}\, \frac{R_{ext}^3 - R_{int}^3}{3} \tag{20}$$

where p is the contact pressure and S is the contact area. The regularised friction coefficient μ_R is a function of the relative angular velocity $\omega_{rel} = (\omega_B - \omega_A) \cdot \boldsymbol{n}$ and is defined as

$$\mu_R(\omega_{rel}) = \begin{cases} \mu_{dyn}\left(2 - \frac{|\omega_{rel}|}{\epsilon_\omega}\right)\frac{\omega_{rel}}{\epsilon_\omega}, & |\omega_{rel}| < \epsilon_\omega; \\ \mu_{dyn}\,\frac{\omega_{rel}}{|\omega_{rel}|}, & |\omega_{rel}| \geqslant \epsilon_\omega. \end{cases} \tag{21}$$

The parameter ϵ_ω gives the value of relative rotation velocity below which the friction effect is assumed negligible, while μ_{dyn} is the dynamic friction

Table 1. Comparison of torque distribution ratios for the four working modes of the type C TORSEN.

TDR	Mode 1 Drive bias to rear	Mode 2 Coast bias to rear	Mode 3 Drive bias to front	Mode 4 Coast bias to front
Experimental	4.02	2.82	1.57	1.62
Continuous impact model	3.89	2.92	1.53	1.66
Error (%)	3.23	3.55	2.55	2.47
Squeeze film model	3.95	2.95	1.49	1.6
Error (%)	1.74	4.61	5.10	1.23

coefficient. This regularised friction function is introduced to avoid the numerical inconveniences (loss of convergence) induced by the discontinuities in friction torque at the instants of reversing the relative rotation velocity.

Rigid contacts between gear wheels and thrust washers of the type C TORSEN differential

The global multibody model of the type C TORSEN differential mainly includes 15 rigid bodies, 8 gear pairs, 4 hinges and 1 screw joint. The contacts between the thrust washers and the rim faces of the gear wheels are modelled by five frictional contact elements defined between two rigid planar rings as presented in this paper.

The contact elements as well as the gear pair model introduce non-symmetric terms in the tangent iteration matrix. Therefore, a non-symmetric solution algorithm has to be used to solve the equation system. In order to adapt the time step size according to the dynamic behaviour of the system during the impact times, an automatic time stepping strategy is used.[8]

In a first step, in order to validate the differential model and check its accuracy, the numerical results have been compared with measurements on an experimental test bench provided by the JTEKT TORSEN Company. To this purpose, the test bench configuration has been reproduced virtually. Contrarily to the operation in a vehicle, the housing does not rotate during the test. It is nevertheless possible to observe the four working modes since the locking effect of TORSEN differentials is due to relative motion and to the forces between the output shafts and the housing.

The setup of these tests consists in applying a torque on one output shaft of the differential, whereas the rotation speed of the second one is prescribed, which is equivalent to apply a resisting torque, and the housing (which is normally the input shaft in a vehicle) is kept fixed as said previously. The four working modes of the differential are activated according to the relative sign of the torque and the rotation velocity on both output shafts. The global

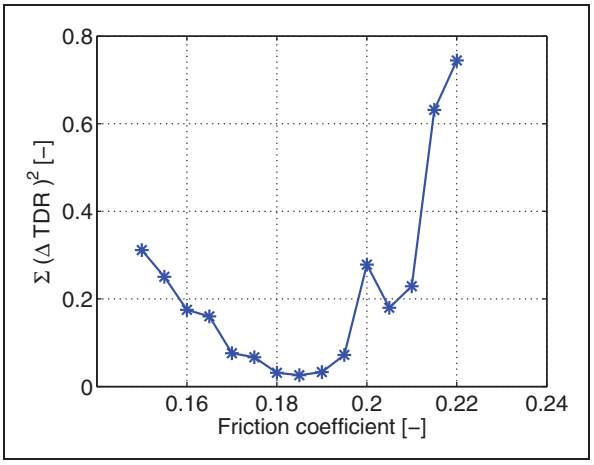

Figure 4. Axial displacement of the sun gear.

validation of the multibody model is achieved by computing the torque ratio between the two output shafts. ThisTDR is a specific index for each working mode of the differential. Table 1 shows the good agreement between the experimental TDR values and the results provided by the numerical simulation since the error is lower than 5% for the four working modes.

Each planet gear is free to move inside a cavity in the housing. This complex joint between the planet gear and the housing is simply modelled as a hinge. The friction forces occurring between the tooth heads of the planet gears and the cavities in the housing where they are contained, are represented by a friction torque along the axis of this hinge. Owing to the significant difference between a hinge model and the actual joint, the value of the friction coefficient in the hinge joint is difficult to assess, and it was identified experimentally as explained later on.

Figures 4 and 5 illustrate the dynamic simulation of the model when the torque applied on the sun gear changes its sign, which leads to quick switches between the working modes of the differential with torque biasing to the front axle. Due to the helical meshing, the sun gear undergoes an axial displacement as soon as the sign of the torque applied on the planet gear changes (see Figure 4(a)). The zoom around the second axial displacement represented in Figure4(b) shows some rebounds of the sun gear

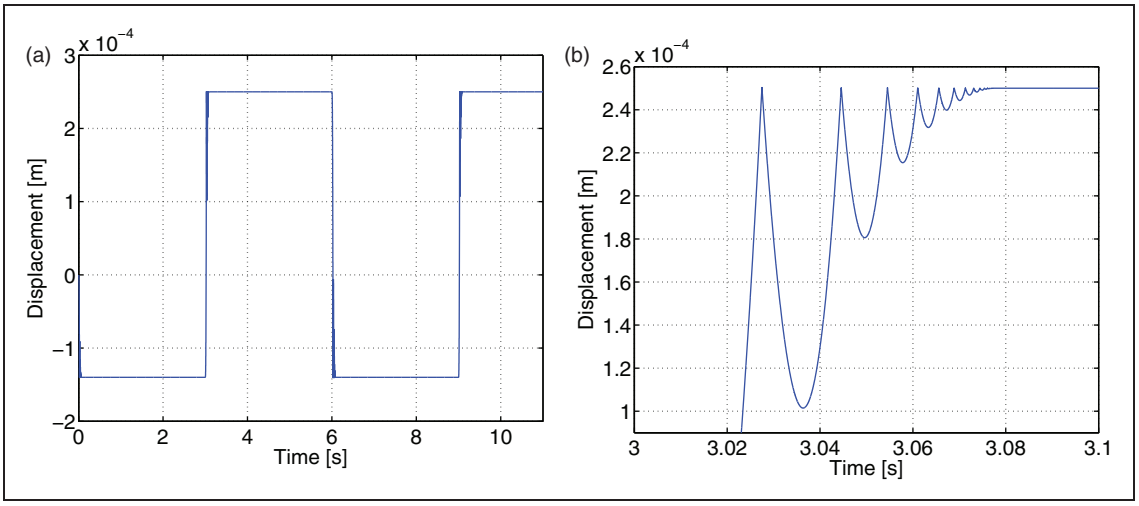

Figure 5. Hysteresis loop representing the kinetic energy loss at each impact between the gear wheel and the thrust washers.

against the thrust washer before reaching a closed contact configuration. The magnitude and the frequency of these rebounds depend on the value of the contact stiffness ($k_p = 10^{10}$ N/m) and the restitution coefficient ($e = 0.8$). The contact stiffness was selected to get a penetration which is in the order of one thousandth of axial displacement of the sun gear, while a restitution coefficient of 0.8 was judged admissible for this impact.

In order to determine the value of the friction coefficient in the hinge joint between planet gears and the housing, a parametric study has been performed. The least squares criterion has been used to find the best friction coefficient, i.e. the value for which the sum of squared differences between experimental and simulated TDR for the four operation modes is minimum (see Table 1). Figure 6 shows that a value of the friction coefficient of 0.185 leads to the model with the closest TDR values compared to the experimental data. We remark that the friction coefficient of these hinge joints is the only parameter that is fitted in order to match the TDR values. The values of the other parameters are imposed by the physics of the problem. The accordance of numerical TDRs with respect to the experimental data shows the accuracy of the MBS model of the TORSEN differential while only one parameter has been adjusted.

As said before, the rebounds shown in Figure 4(b) are related to the value of the contact stiffness, and evidenced a very sharp discontinuity in velocity. In order to solve these impacts accurately, the integrator automatically selected a very small value of the time step during the penetration phase (more or less 10 time steps are performed during each penetration phase as seen in Figure 5). If a larger time step were used, important errors in energy and momentum conservation would appear. Therefore, this simulation is very costly, because of the rigid/rigid contact modelling hypothesis for these parts of the model.

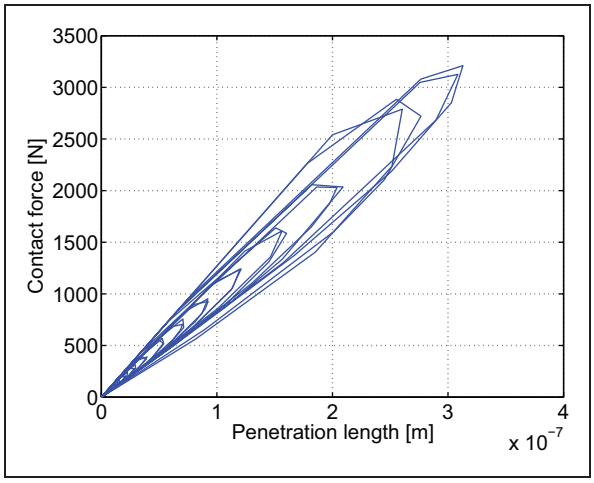

Figure 6. Parametric study: influence of the friction coefficient in hinge joints on the sum of squared differences between experimental and computed TDRs for the four operation modes.

In the present application, the determination of the coefficient of restitution and the contact stiffness can hardly be based on physical data and it thus remains an inherent difficulty of the continuous impact modelling approach. This motivates the development of a more physical approach using a squeeze film contact model.

Squeeze film contact model

Lubrication is required in order to have a proper operation of many transmission devices. The oil film allows to evacuate material fragments and the heat generated by friction. Wear is greatly reduced when mechanisms are adequately lubricated. Therefore, the contact properties are significantly influenced by the presence of the lubricant.

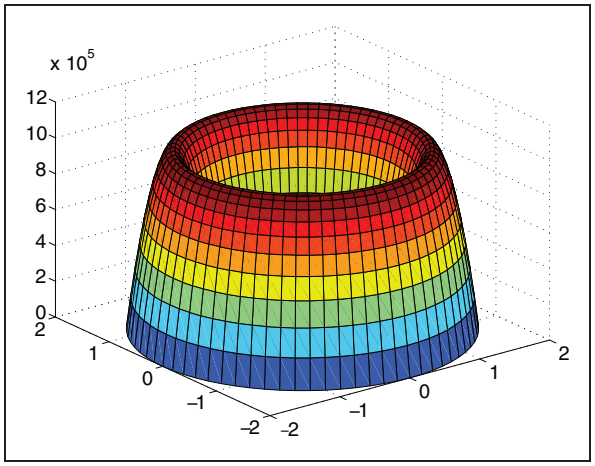

Figure 7. Oil pressure profile for a squeeze film between two plane rings.

Numerous formulations are available in the literature to model the lubricated contacts and account for several effects.[20,21] In the context of multibody systems, the lubrication is often modelled in a more global way.[22–24] In this paper, the goal of the lubrication model is only to be able to represent the damping behaviour of the oil film between two mechanical parts. This small damper tends to slow down the contacting bodies before the contact establishment and therefore reduces the impact impulse since the relative velocity is lower at the impact time.

This section describes a simple squeeze film model allowing to describe the damping effect due to the lubrication film when two bodies are approaching. Poiseuille flow in the radial direction is assumed, particularised to the geometric configuration of the contact between two planar rings, while Couette flow is considered in the tangential direction. The assumptions are similar to those leading to the Reynolds equation and can be summarized as follows: the flow is fully developed, the fluid is Newtonian, incompressible and isothermal in steady state; the flow is laminar and parallel to the film walls; the film thickness h_{sf} is much smaller than the radii of the rings (R_{int}, R_{ext}) which always remain parallel; the pressure p is constant in the normal direction z; no slip conditions at the walls are assumed; the inertia terms and gravity forces are neglected.

Owing to the introduced hypotheses and by considering v_r/r^2 is negligible compared to $\partial^2 v_r/\partial z^2$, the radial component of the simplified Navier–Stokes equation (momentum conservation) reduces to

$$\frac{\partial p}{\partial r} = \mu_{vis} \frac{\partial^2 v_r}{\partial z^2} \tag{22}$$

where μ_{vis} is the dynamic viscosity of the lubricating oil and v_r is the fluid velocity in the radial direction.

The continuity equation in cylindrical coordinates is formulated as

$$\frac{1}{r}\frac{\partial}{\partial r}(r\, v_r) + \frac{\partial v_z}{\partial z} = 0 \tag{23}$$

After double integration of equation (22) in the axial direction (z-axis), and by using the no slip boundary conditions at the walls, i.e. $v_r = 0$ in $z = 0$ and $z = h_{sf}$, we get the expression of the velocity at a given radial position r, which has a parabolic profile in the z-direction and a sign opposite to the pressure gradient $\partial p/\partial r$

$$v_r = -\frac{1}{2\mu_{vis}}\frac{\partial p}{\partial r}\left(h_{sf}\, z - z^2\right) \tag{24}$$

After having replaced the velocity profile (24) into equation (23), the continuity equation is integrated in the longitudinal direction between $z = 0$ and $z = h_{sf}$ to get

$$-\frac{\partial}{\partial r}\left(r\frac{1}{2\mu_{vis}}\frac{\partial p}{\partial r}\right)\frac{h_{sf}^3}{6} + r\dot{h}_{sf} = 0 \tag{25}$$

This last expression is then integrated in the radial direction, and by using the boundary conditions $p(R_{int}) = p(R_{ext}) = 0$, the expression of the fluid pressure $p(r)$ can be computed. Finally, the global force applied by the squeeze film on the two rings results from the integration of the fluid pressure over the ring area S

$$f_{sf} = \int\int_S p(r)\, \mathrm{d}S \tag{26}$$

In summary, the force applied on the two rings can be reduced to the expression

$$f_{sf}(h_{sf}, \dot{h}_{sf}) = -\frac{3}{2}\pi\mu_{vis} G\, \frac{\dot{h}_{sf}}{h_{sf}^3} \tag{27}$$

where the constant G is defined in terms of the internal and external ring radius

$$G = \left(R_{int}^2 - R_{ext}^2\right)\left(\frac{R_{ext}^2 - R_{int}^2}{\ln\frac{R_{ext}}{R_{int}}} - 2R_{ext}^2\right) - \left(R_{ext}^2 - R_{int}^2\right)^2 \tag{28}$$

The expression (27) of the contact force enables to conclude that the developed squeeze film model has the behaviour of a nonlinear damper ($f_{sf} = 0$ when $\dot{h}_{sf} = 0$). Nevertheless, it acts as a nonlinear spring with a tangent stiffness when $\dot{h}_{sf} \neq 0$.

The viscosity of the lubricating oil introduces a viscous resistance which tries to slow down the relative rotation between the two rings. This viscous resistance

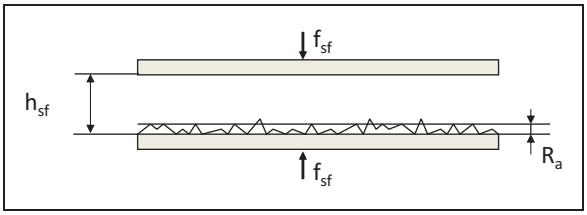

Figure 8. The roughness of the plates limits the thickness to a minimal value.

is introduced in the model by means of a torque along the z-axis

$$T_{vis} = \int_S \frac{\mu_{vis}\ \omega\ r^2}{h_{sf}}\,\mathrm{d}S = 2\pi\ \frac{\mu_{vis}\ \omega}{h_{sf}}\ \frac{R_{ext}^4 - R_{int}^4}{4} \quad (29)$$

where ω is the relative rotation velocity in the longitudinal direction.

The force introduced by the squeeze film effect is opposed to the relative bodies motion, trying to separate them when the walls are approaching and to avoid separation when the two walls are pulling away. When the film thickness tends to zero, the predicted force tends to infinity, which is not physically realistic. In fact, the roughness on the plate surface and geometric imperfections (e.g. planarity and angular tolerances) are such that the lubricating film thickness can never decrease below a limit value for which contacts can be assumed to appear between plates asperities (see Figure 8). Also, note that the conditions for fully developed flow would be no longer valid when h_{sf} gets close to roughness. Therefore, when the film thickness becomes lower than the arithmetic roughness R_a, a contact force between the rigid walls is added to the squeeze film model. The latter is simply modelled by a linear penalty method, where k_p is the global contact stiffness of the two plates.

$$f_{con}(h_{sf}) = \begin{cases} 0 & \text{if} \quad h_{sf} \geqslant R_a \\ k_p\ (h_{sf} - R_a) & \text{if} \quad h_{sf} < R_a \end{cases} \quad (30)$$

Moreover, this additional contact force allows to avoid the ill conditioning of the squeeze film model, when h_{sf} and $\dot{h}_{sf}$ are simultaneously close to zero (see equation (27)).

The friction induced by the contact between the two rings is taken into account in the model through a friction torque in the direction z

$$T_{fr} = \begin{cases} 0 & \text{if} \quad h_{sf} \geqslant R_a \\ \frac{2}{3}\ \mu_R\, f_{con}\ \frac{R_{ext}^3 - R_{int}^3}{R_{ext}^2 - R_{int}^2} & \text{if} \quad h_{sf} < R_a \end{cases} \quad (31)$$

with μ_R the regularised friction coefficient (see equation (21)).

In order to include the proposed squeeze film model within a dynamic multibody system formulated with finite element coordinates, the same kinematic description developed for the continuous impact model can be used (see Figure 2). In the material frame attached to node A, the forces (14) acting between the two rings are expressed as

$$\boldsymbol{f}_t = \begin{Bmatrix} f_{sf} + f_{con} \\ 0 \\ 0 \end{Bmatrix}, \quad \boldsymbol{f}_r = \begin{Bmatrix} T_{vis} + T_{fr} \\ 0 \\ 0 \end{Bmatrix} \quad (32)$$

if the first axis of the material frame attached to nodes A and B is oriented along the normal direction of the thrust washers.

Lubricated contact inside the type C TORSEN differential

The TORSEN differentials are usually located inside the casing of the gear box. The holes drilled in the housing and the case of the differential enable the flow of the lubricating oil through the differential. The narrow gap between the gear wheels and the thrust washers is then filled by the lubricant that influences significantly the properties and the dynamic response of the various contacts. For instance, the relative velocity when the two bodies enter in contact is highly reduced since the film of lubricant acts as a damper; hence, the impacts are moderated or even avoided.

The five rigid contact conditions based on the continuous impact model included in the model of the type C TORSEN differential are now replaced by the combined squeeze film – frictional contact model. Since the squeeze film formulation enables to smooth the discontinuities induced by unilateral contacts, the number of contact conditions included in the multibody system model can be increased without degrading the convergence properties. Therefore, the hinge joints modelling the connection between each planet gear and the housing can be replaced by a cylindrical joint and two contact conditions modelling the contacts between the lateral faces of the planet gears and the housing or the case. The friction torques due to these contacts also contribute to the global torque transfer and the locking behaviour of the differential. It is the reason why their introduction in the model could improve the accuracy of the differential model. Since the geometric configuration of these contacts is similar to the other contacts (i.e. ring contact area), the same squeeze film contact formulation can be used. Thanks to the squeeze film modelling, the simulation of the full type C TORSEN differential model including now 14 contact conditions presents an enhanced robustness.

The dynamic behaviour of the differential in the vehicle configuration is reproduced by applying a

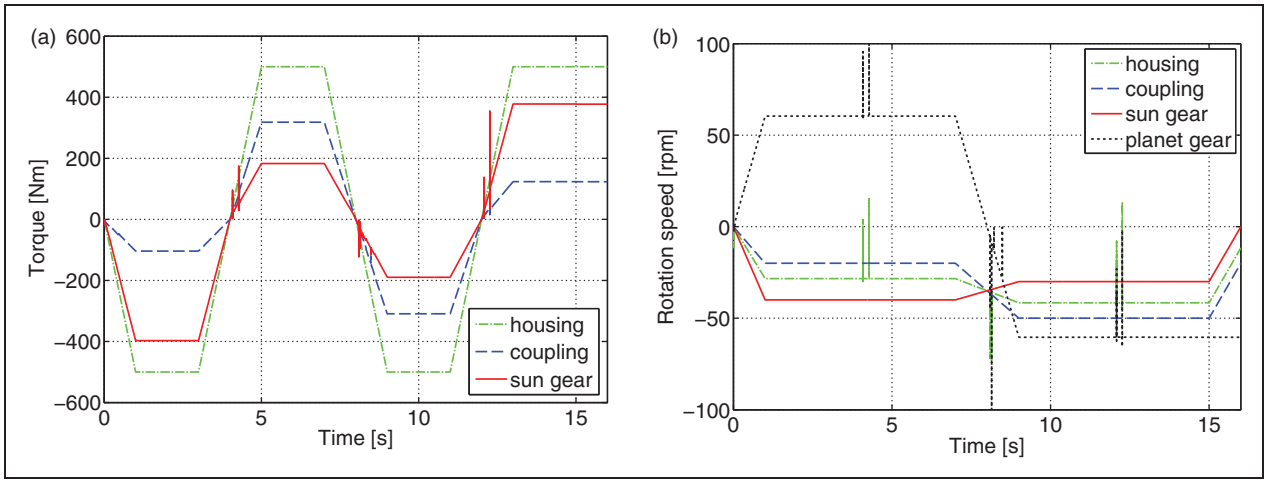

Figure 9. Torque and angular velocity of the various gear wheels.

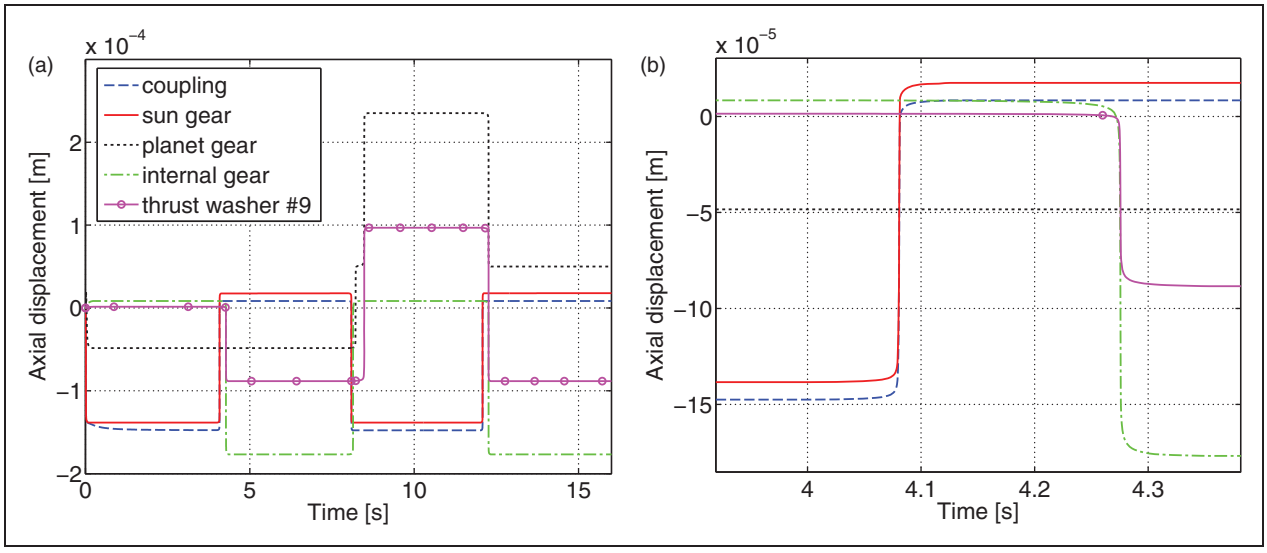

Figure 10. Axial displacement of bodies inside the differential.

torque on the housing while the rotation speeds of the two differential outputs (sun gear and coupling) are prescribed (see Figure 9 for the time evolution given to these three quantities). With this set of load cases, the drive to rear mode is active at the beginning of the simulation, the coast to front and drive to front modes are observed during the periods $t = [4; 8]$ s and $t = [8; 12]$ s, respectively, and the coast to rear mode at the end of the simulation.

Figure 10 shows the displacements in the axial direction of the gear wheels and the thrust washer #9 inside the differential. Each working mode corresponds to a different configuration of this set of bodies.

The damping effect of the squeeze film model can be observed on the displacement curves (Figure 10(a)): the gear wheels are slowed down before the establishment of contact against the thrust washers. In this way, the impacts between these rigid bodies are avoided or at least greatly reduced. The sticking effect which acts against the separation of the contacting bodies is also visible and explains why some gear wheels move sometimes with a small delay at the switching time between two working modes. The little step on the displacement of the planet gears when the drive to front mode is activated at $t = 8$ s is also due to this sticking phenomenon.

The squeeze film produces a significant force during the transient phases between two working modes but this force vanishes when the bodies are in closed contact situation. This is due to the fact that the squeeze film force is directly proportional to the velocity of the film thickness (see equation (27)). The latter is null when the lubricating film has reached a steady state thickness slightly lower than the arithmetic roughness. In the normal operation of a vehicle,

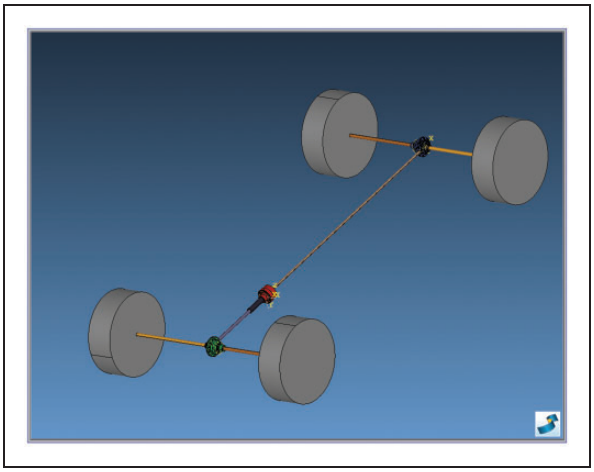

Figure 11. Four-wheel drive simplified vehicle model with three differentials.

the difference of rotation speed between the two axles is not tremendous so that the magnitude of the viscous torques is insignificant compared with the friction torques.

Due to the lower axial force transmitted by the contacts on the top and bottom faces of the planet gears and the smaller radius of their contact area, the related friction torques are much lower than the friction torques of the other contacts with the thrust washers. Nevertheless, the axial motions of the planet gears enable to account for the contact between the thrust washer #9 and the internal gear in the drive to front mode (third mode). The friction torque involved by this contact is sizeable and modifies the torque distribution in the differential. This phenomenon could not be represented using a differential model with locking of the planet gears.

Since additional friction forces have been added in the system due to the planet gear displacements, the friction coefficient in the hinge joints between the planet gears and the housing has to be readjusted if necessary. From a parametric study similar to Figure 6, the friction coefficient leading to the best agreement between the numerical and experimental TDR values is determined equal to 0.17.

The resisting torques allowing to impose the rotation speed of the sun gear and the coupling are depicted in Figure 9(a). The gap between these two curves is a measure of the locking rate of TORSEN differentials for each working mode. The TDRs computed from these torque curves are given in Table 1. Similarly to the differential model using the rigid/flexible contact model or the continuous impact model, the numerical TDR values agree with the experimental data since for all modes the relative error is lower than 5%. However, the model including the squeeze film contacts is more robust and can be simulated using larger time steps which reduce the CPU time by a factor of 100 for the proposed simulation.

We remark that the particular boundary conditions imposed in this analysis are at the origin of the torque and velocity pikes observed in Figure 9. In fact, an input torque is imposed on the housing, while rotation speeds are imposed at the output shafts. At the time instants at which the inner bodies displace axially, the planet gears and the housing accelerate and when contact is reestablished, a torque peak appears. In a real situation, this phenomenon is mitigated by the rotary inertia of the input axis and of the engine.

Interaction of the differential with the vehicle dynamics

The TORSEN differentials strongly interact with the other transmission components (e.g. the gear box) and the other vehicle subsystems such as the suspension mechanisms. Therefore, there is a need to develop integrated simulations of differentials together with the vehicle dynamics.

As final application of this paper, a global four-wheel drive vehicle equipped with three TORSEN differentials has been modelled (Figure 11). The central differential is the type C TORSEN studied in this work, whereas the front and the rear differentials are the type B TORSEN. The working principle of the latter is similar to the type C and its multibody model is described in Virlez.[16]

The objective of this model is to observe the distribution of the engine torque between the four wheels. In this context, a simplified vehicle model where the car body is modelled by a lumped mass is considered. The suspensions and the steering mechanisms are ignored. The differentials are attached to the vehicle frame with hinge joints. In order to connect the central differential with the front and rear differentials, conical gear pairs are introduced in the model. The drive shafts linked to the inputs and the outputs of the differentials are represented by rigid bodies connected to wheel models (Pacejka's magic formula)[25]. The vehicle is driven by a torque applied on the housing of the central differential.

In order to study the torque transfers induced by the limited slip behaviour of the three TORSEN differentials, quite different grip conditions have been chosen for each wheel of the vehicle, even if it is not very realistic. The rear right wheel has a good adherence, with parameters given by the Pacejka's wheel model. The ground in contact with the other wheels has a lower adherence, with its properties being given by scaling the grip potential of the rear right wheel with a factor equal to 0.5 for the rear left wheel, 0.4 for the front right wheel and 0.1 for the front left wheel.

The torque distribution between the four driving wheels is illustrated in Figure 12(a). Since a driving torque is applied on the central differential and the rear wheels have a better adherence than the front wheels, the drive to rear mode of the type C

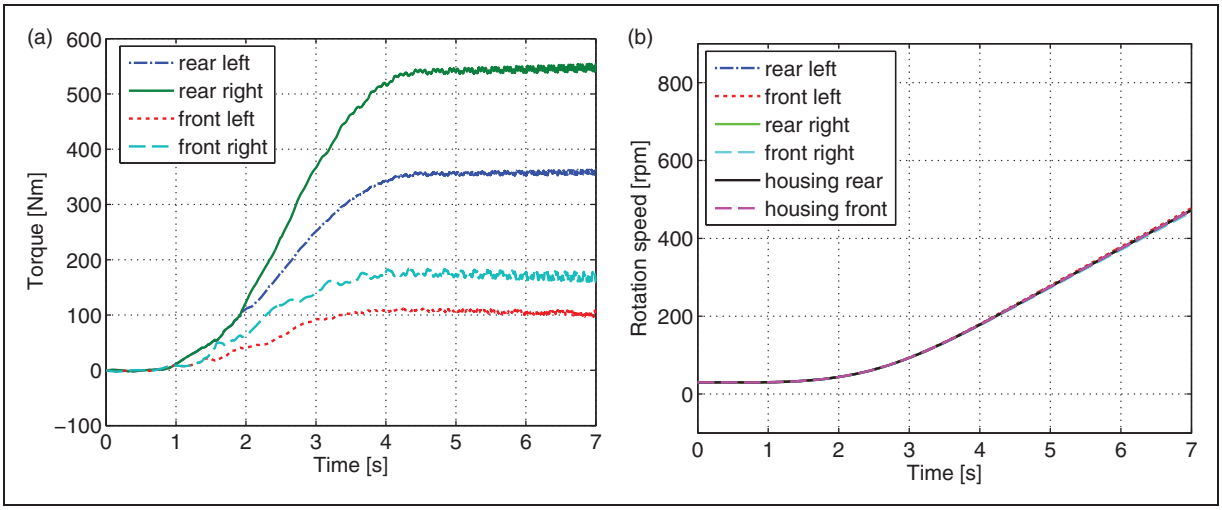

Figure 12. Distribution of the driving torque and the rotation speed between the four driving wheels having a different friction coefficient (maximum torque = 300 N/m).

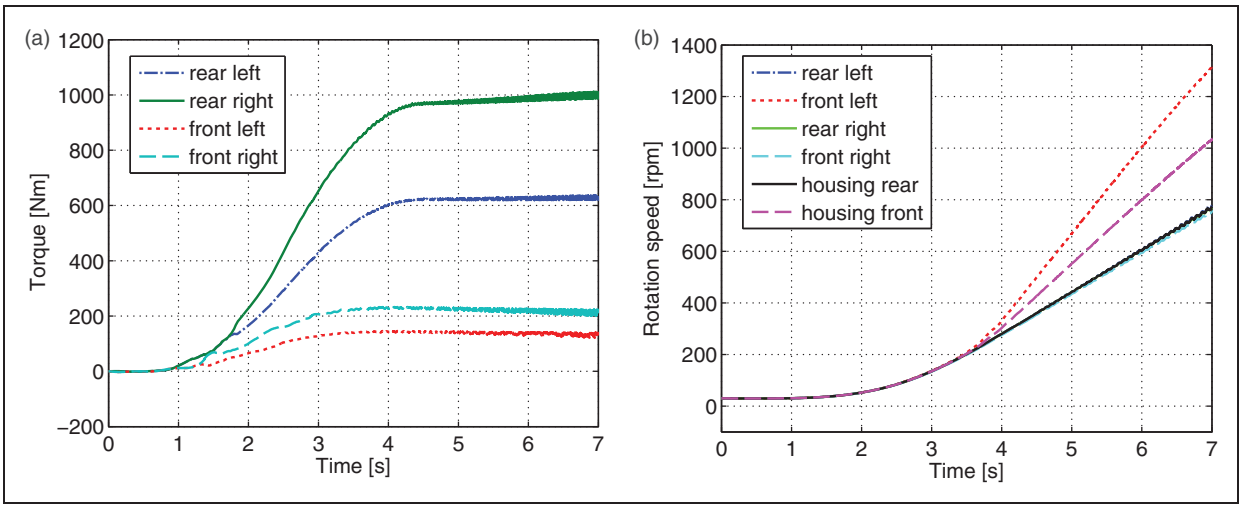

Figure 13. Distribution of the driving torque and the rotation speed between the four driving wheels having a different friction coefficient (maximum torque = 500 N/m).

TORSEN differential is activated. Therefore, the rear wheels receive more torque than the front wheels. It can be verified that the torque ratio between the front axle and the rear axle matches the TDR value of the drive to rear mode as given in Table 1. Likewise, both front and rear differentials provide more torque to the right wheels because the right lane has a better adherence.

Figure 12(b) depicts the angular velocities of the planet gears and the four wheels. The three differentials are nearly locked since all the wheels almost rotate at the same speed and the planet gears have only a small angular velocity. Let us remark that the purely closed configuration of TORSEN differentials corresponds to no relative sliding inside differential. Nevertheless, a small sliding is still observed in the proposed numerical model because of the regularisation of the friction coefficients.

The model can also represent the fully open configuration. To this end, the same system has been simulated with a higher driving torque, the maximal value of the torque amounting to 500 Nm instead of 300 Nm. The torque curves keep similar time evolution as illustrated in Figure 13(a) but the rotation speeds are significantly different (Figure13(b) compared with Figure12(b)). Indeed, the potential of adherence is exceeded for the front left wheel and results in the spinning of this wheel. The other wheels have almost the same speed, whereas the housing of the front differential rotates at a mean velocity between the right and the left front wheels. The planet gears of the central and the front differential turn much quicker than in

the previous simulation, which is representative of the fully open status of both differentials.

Conclusion

The developments presented in this paper contribute to the dynamic modelling of mechanical transmissions devices submitted to unilateral contacts. The TORSEN differential is a complex industrial system whose modelling encounters several difficulties such as impact, friction or backlash between gear teeth.

The construction of a global multibody model of the type C TORSEN differential with the commercial simulation code SAMCEF MECANO has pointed out the need for contact models between rigid bodies, able to deal with the discontinuities produced by impact. Indeed, at the switching time between two working modes, the gear wheels undergo a quick axial displacement before entering in contact with the thrust washers.

The 3D formulation to describe the kinematics of contact between two rigid bodies represented by two nodes has been particularised in this paper to the geometric configuration of two planar rings remaining parallel and coaxial.

In a first step, the magnitude of the normal contact force was computed by means of a continuous impact model. This penalty method uses a restitution coefficient in order to account for the kinetic energy loss during impact. The friction torque is based on a regularisation method to avoid the numerical discontinuity between the stick and the slip phases.

In a second step, the influence of the lubrication in the narrow gap between the two rigid bodies in intermittent contact is added in the contact model. The normal force produced by the squeeze film takes the form of a nonlinear damper and has a compact expression thanks to a set of geometric and physical hypotheses. When the thickness of the oil film is lower than the arithmetic roughness of the walls, contact occurs between the two metallic bodies which is also modelled by a penalty method. In addition to the contact forces in the normal direction, the friction torques in the tangential plane are also included in the model.

The continuous impact model and the squeeze film model have been tested in the type C TORSEN differential model to represent the unilateral contact conditions between the thrust washers and rim faces of the gear wheels. In both cases, the comparison of the TDR of the four working modes with experimental data allows to validate the model in a global way. The modelling of the squeeze film enables to better describe the physical behaviour of the differential and also leads to an increased numerical robustness and a reduced computational time since larger time steps can be used.

Finally, three TORSEN differential models including the combined squeeze film – contact model have been assembled to represent the driveline of a simplified four-wheel drive vehicle. This model shows the feasibility of the modelling approach adopted in order to simulate the interactions between transmission components and the vehicle dynamics.

Acknowledgements

The authors wish to thank Mr. Nicolas Poulet (JTEKT TORSEN EUROPE S.A.) for kindly providing the technical data needed to develop the model of the differential.

Declaration of conflicting interests

The author(s) declared no potential conflicts of interest with respect to the research, authorship, and/or publication of this article.

Funding

The author(s) disclosed receipt of the following financial support for the research, authorship, and/or publication of this article: the first author, Geoffrey Virlez, would like to acknowledge the Belgian National Fund for Scientific research (FRIA) for its financial support.

References

1. Ma ZD and Perkins N. An efficient multibody dynamics model for internal combustion engine systems. *Multibody Syst Dyn* 2003; 10: 363–391.
2. Blundell M and Harty D. *The multibody systems approach to vehicle dynamics*. Oxford: Elsevier Butterworth-Heinemann Publications, 2004.
3. Ziegler P and Eberhard P. *Simulation of gear hammering with a fully elastic model. Non-smooth problems in vehicle systems dynamics*. Berlin Heidelberg: Springer, 2010, pp.195–207.
4. LMS SAMTECH SAMCEF MECANO. *V16 – user's and installation manual*. A SIEMENS business, www.plm.automation.siemens.com/fr_be/products/lms/samtech/samcef-solver-suite/index.shtml, (2014, accessed 27 February 2016).
5. Flores P and Lankarani H. Spatial rigid-multibody systems with lubricated spherical clearance joints: modeling and simulation. *Nonlinear Dynam* 2010; 60: 99–114, http://dx.doi.org/10.1007/s11071-009-9583-z. (accessed 27 February 2016).
6. Theodossiades S, Tangasawi O and Rahnejat H. Gear teeth impacts in hydrodynamic conjunctions promoting idle gear rattle. *J Sound Vibr* 2007; 303: 632–658.
7. Blockmans B, Tamarozzi T, Naets F, et al. A nonlinear parametric model reduction method for efficient gear contact simulations. *Int J Numer Meth Eng* 2015; 102: 1162–1191.
8. Géradin M and Cardona A. *Flexible multibody dynamics: a finite element approach*. New York, NY: John Wiley & Sons, 2001.
9. Chung J and Hulbert G. A time integration algorithm for structural dynamics with improved numerical dissipation: the generalized-α method. *ASME J Appl Mech* 1993; 60: 371–375.
10. Arnold M and Brüls O. Convergence of the generalized-α scheme for constrained mechanical systems. *Multibody Syst Dyn* 2007; 18: 185–202.
11. Cardona A. Flexible three dimensional gear modelling. *Eur J Comput Mech* 1995; 268: 663–691.

12. Cardona A. Three-dimensional gears modelling in multibody systems analysis. *Int J Numer Meth Eng* 1997; 40: 357–381.
13. Jetteur P. Contact between flexible bodies in nonlinear analysis, using Lagrange multipliers. In: *International conference on engineering computational technology*, Vol VII, Leuven, Belgium, 6 September 2000, pp. 257–261. Edinburgh: Civil-Comp Press, ROYAUME-UNI.
14. Virlez G, Brüls O, Poulet N et al. Simulation of differentials in four-wheel drive vehicles using multibody dynamics. In: *Proceedings of the ASME 2011 international design engineering technical conferences computers and information in engineering conference IDETC/CIE 2011*, 29–31August, 2011, Washington, DC, USA.
15. Virlez G, Brüls O, Poulet N, et al. Modelling of contact between stiff bodies in automotive transmission systems. In: Jean-Claude S and Paul F (eds) *Computational methods in applied sciences*, volume Multibody dynamics: computational methods and applications. Springer, 2013, pp.193–214. Netherlands: Springer.
16. Virlez G. *Multibody modelling of mechanical transmission systems in vehicle dynamics*. PhD Thesis, University of Liège, Belgium, 2014.
17. Lankarani H. *Canonical equations of motion and estimation of parameters in the analysis of impact problems*. PhD Thesis, University of Arizona, USA, 1988.
18. Lankarani H and Nikravesh P. Continuous contact force models for impact analysis in multibody analysis. *Nonlinear Dyn* 1994; 5: 193–207.
19. Flores P, Machado M, Silva M, et al. On the continuous contact force models for soft materials in multibody dynamics. *Multibody Syst Dyn* 2011; 25: 357–375.
20. Brunetire N and Tournerie B. Numerical analysis of a surface-textured mechanical seal operating in mixed lubrication regime. *Tribol Int* 2012; 49: 80–89. www.sciencedirect.com/science/article/pii/S0301679X12000059 (accessed 27 February 2016).
21. Yang B and Laursen TA. A mortar-finite element approach to lubricated contact problems. *Comput Meth Appl Mech Eng* 2009; 198: 3656–3669. www.sciencedirect.com/science/article/pii/S0045782509002321 (accessed 27 February 2016).
22. Khonsari M. On the modeling of multi-body interaction problems in tribology. *Wear* 1997; 207(12): 55–62. www.sciencedirect.com/science/article/pii/S0043164896074832 (accessed 27 February 2016).
23. Karagiannis I, Theodossiades S and Rahnejat H. On the dynamics of lubricated hypoid gears. *MechMach Theory* 2012; 48: 94–120.
24. Tian Q, Liu C, Machado M, et al. A new model for dry and lubricated cylindrical joints with clearance in spatial flexible multibody systems. *Nonlinear Dyn* 2011; 64: 25–47.
25. Bakker E, Pacejka HB and Lidner L. *A new tire model with an application in vehicle dynamics studies*. SAE Technical Paper 890087, 1989.